

Monte Carlo analysis of total damping and flutter speed of a long span bridge: Effects of structural and aerodynamic uncertainties

T. Argentini*, A. Pagani, D. Rocchi, A. Zasso

Politecnico di Milano, Department of Mechanical Engineering, via La Masa 1, 20156 Milano, Italy

Article history:

Received 9 September 2013

Received in revised form

12 February 2014

Accepted 22 February 2014

1. Introduction

The continuous progress in knowledge and technology has let engineers design suspension bridges with increasingly longer spans. A major concern for such slender structures is that they suffer from aeroelastic instabilities caused by the self-excited aerodynamic forces acting on the deck. While the risk of torsional divergence can be avoided by a careful aerodynamic design of the deck section, flutter instability still remains a critical aspect that involves both the structural and the aerodynamic characteristic of the bridge: evaluating and predicting the aeroelastic performances of the bridge during construction and *in service* states is therefore

a crucial point of its design (e.g. [Diana et al., 1995, 2013b](#); [Argentini et al., 2013, 2011](#); [Ge, 2011](#)).

Since the first aeroelastic studies of civil structures, the problem of stability has been studied from a deterministic point of view; nowadays, this approach is the starting point of probabilistic analyses that take into account the uncertainties of the parameters involved. Such an approach is a more powerful design tool, since it supports deterministic results with confidence intervals (e.g. [Jakobsen and Tanaka, 2003](#)).

Within this framework, researchers have dealt with the reliability of deterministic flutter prediction for several years (e.g. [Bucher and Lin, 1988](#); [Prenninger et al., 1990](#); [Ostenfeld-Rosenthal et al., 1992](#); [Pourzeynail, 2002](#)). The most used and developed approaches are the *First* and the *Second Order Reliability* method (as proposed by [Cheng et al., 2005](#); [Ge et al., 2000](#); [Cheng and Li, 2009](#); [Baldomir et al., 2011](#); [Kiureghian, 2005](#)), and the Monte-Carlo method ([Bartoli and Mannini, 2005](#); [Mannini and](#)

* Corresponding author.

E-mail address: tommaso.argentini@polimi.it (T. Argentini).

Bartoli, 2010). The former methods manage the reliability problem considering a linearized objective function, while the latter allows one to numerically obtain the statistical distribution of the target parameter.

All the cited works consider the critical flutter speed as the key parameter of the reliability analysis, however the critical flutter speed is not a unique index for the assessment of the safety of the structure against wind loads. Besides the flutter speed, the trend of the total damping of the structure (ζ_{tot}) as a function of the mean wind velocity is a complementary safety index that allows one to assess the aeroelastic behavior of a bridge over a wide range of operating conditions.

As a matter of fact, the critical wind speed ($V_{flutter}$) is in general larger than the maximum wind speed the structure is expected to withstand in its life period, that is called design velocity (V_{design}). This wind speed has a large return period (or a low probability of occurrence): usually, the structure faces wind speeds that are lower than the design speed and with a shorter return period. Thus it is important to assess the safety of a bridge also for wind velocities that are more probable than the design velocity.

To this end, the total damping of the structure (intended as the sum of the structural and aerodynamic damping, $\zeta_{tot} = \zeta_{aero} + \zeta_{str}$) is a relevant safety index. Therefore, the uncertainties on the aeroelastic stability of the structure should be investigated not only at extreme conditions, but also in the operating ones. In order to do this, in this paper, the probabilistic study of the flutter speed is complemented with a probabilistic analysis of the total damping of the bridge for several operating wind velocities.

To better explain why the trend of total damping is an important safety index, we propose the following example in which we compare two different design solutions having the same critical flutter speed, but very different performance at typical *in-service* conditions, as qualitatively sketched in Fig. 1.

For the considered example, two solutions (named A and B) show the typical trends of the total damping parameter that, starting from the structural value (ζ_{str}) in still air, initially increase their value up to a maximum, and then they reverse their slope until the total damping becomes negative (at $V/V_{flutter} = 1$).

If the aerodynamic design is correctly performed, the total damping (ζ_{tot}) should be sufficiently large in all the wind speed range. With reference to Fig. 1, the total damping ζ_{tot} for Solution B is large only in the lower range of wind velocity (around $V/V_{flutter} = 0.2$), and then it decreases up to instability. It is important to have larger values of ζ_{tot} also at high wind speed, as shown by Solution A, in order to have a sufficient safety margin also in the presence of uncertainties on design parameters to prevent undesired instability problem.

The way the Messina Project Technical Specifications deals with the problem is to prescribe minimum threshold for the ζ_{tot} parameters in the range of wind speed from 0 to V_{design} , shown by the rectangular boundaries in Fig. 1. The higher minimum value in the first range is representative of the requirements for a limited buffeting bridge response due to the unsteady turbulent wind conditions. The second limit asks that aerodynamic effects keep on adding dissipation to the structure up to the design speed.

All these considerations make the total damping ζ_{tot} a relevant design index for the safety of the bridge, when aeroelastic effects are present. That is why the propagation of uncertainties and its statistical analysis have to be extended to the total damping instead of referring only to the critical flutter speed, as traditionally done.

With this purpose, the objective of this research paper is to present a methodology to assess the uncertainty of ζ_{tot} in order to evaluate whether possible mismatches between design parameters and actual ones do impact in a critical way on the evolution of the aeroelastic behavior of the structure.

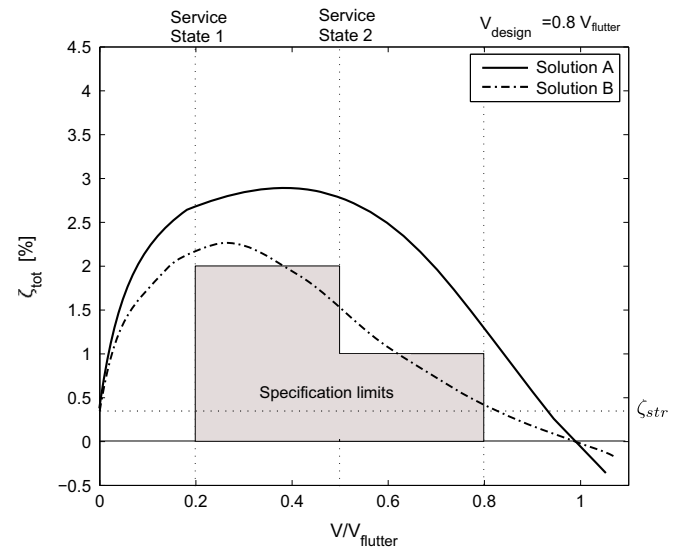


Fig. 1. Total damping as a function of the wind speed (in non-dimensional form).

The Messina suspension bridge (3300 m of main span) is taken as a test case, since for very long span bridges the aeroelastic effects are dominant in the design. Due to the peculiar role played by the aeroelastic coupling of the wind-structure problem in the proposed methodology, even if the analysis procedure is suitable to evaluate the uncertainty effects on fluid-structure interaction of different bridges, the results that will be presented cannot be extended to all suspended bridges because they depend on aerodynamic characteristics and structural properties of the considered structure.

The paper is organized as follows. Section 2 introduces the analysis background: the fluid-structure interaction model; the algorithm used to assess the aeroelastic stability; the Monte-Carlo method; the uncertainties considered in the analysis.

In Section 3 numerical results are presented following these strategies:

- initially, a deterministic approach is used to perform a preliminary investigation to select the most relevant structural and aerodynamic parameters, on the total damping and critical wind speed estimation, by varying each parameter individually.
- Then Monte-Carlo Simulations (MCS) with Hypercube Latin Sampling are run to perform a multivariate analysis considering a simultaneous variation of all the most relevant parameters, previously selected through the deterministic analysis. This procedure allows to have a statistical distribution of the results, as suggested in other works (Matsumoto et al., 1996; Cheng and Li, 2009).
- Specific considerations about the considered test-case are reported.

Finally, conclusions are discussed in Section 4.

2. Analysis background

2.1. Self-excited wind loads

The aeroelastic stability analysis is performed using an iterative multi-modal eigenvalue approach in laminar flow on a complete scheme of the bridge. The aerodynamic forces are modeled using a sectional approach considering their interaction with deck, towers and cable system. To define the aerodynamic forces each bridge

element (tower, deck, and cables) is divided into several rigid sections subjected to a bi-dimensional fluid–structure interaction, that is a widely accepted hypothesis for slender structures.

The mode shapes, the natural frequencies and the modal parameters of the bridge (modal mass and stiffness) in still air are computed through a finite elements scheme of the structure.

Adopting the modal approach, the dynamics of the structure can be written as

$$[M_s^*]\ddot{\underline{q}} + [C_s^*]\dot{\underline{q}} + [K_s^*]\underline{q} = [\Phi]^T \underline{F}_{aero} = \underline{Q}_{aero} \quad (1)$$

where \underline{q} is the vector of the modal coordinates; $[M_s^*]$, $[C_s^*]$ and $[K_s^*]$ are the structural inertial, damping, and stiffness modal matrices of the system, respectively; \underline{Q}_{aero} is the vector of the Lagrangian components of the external aerodynamic forces (\underline{F}_{aero}). Each term of the \underline{F}_{aero} vector is calculated as the virtual work done by the aerodynamic forces acting on the structure due to a unit variation of the corresponding modal coordinate. The evaluation of that virtual work, performed in terms of summation of the contribution of all the considered sections (and all elements), gives rise to generalized forces dependent on the displacement, on the velocity and on the acceleration of each section considered, so that determining state-dependent forces and coupling among the different modes.

As an example, the self-excited unsteady aerodynamic terms of drag, lift and moment acting on the j -th deck section (D_j , L_j , and M_j in Fig. 2) are modeled using the Flutter Derivatives coefficients that were measured with dedicated forced motion tests at the wind tunnel of Politecnico di Milano (Diana et al., 2004, 2013a).

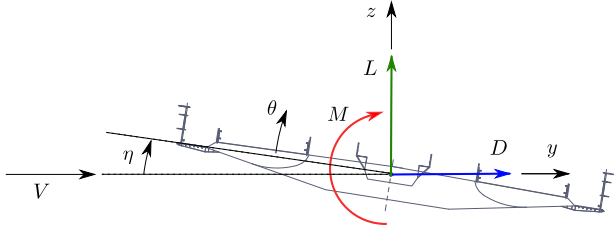
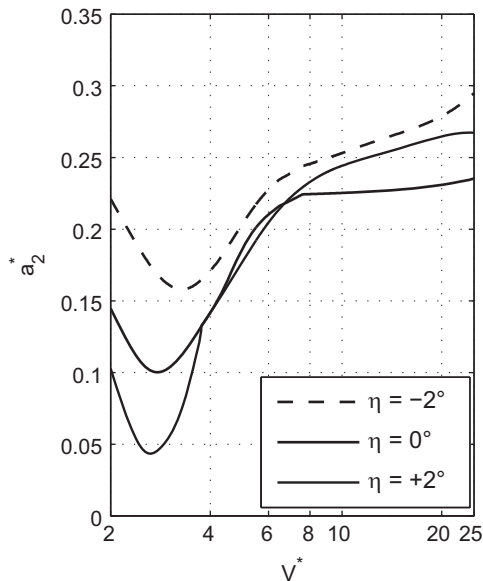


Fig. 2. Sign convention and nomenclature for deck section displacements and aerodynamic forces.



The self-excited forces acting on the generic j -th section are defined, according to the *Politecnico di Milano* convention (see Zasso, 1996), as

$$\begin{bmatrix} D_j \\ L_j \\ M_j \end{bmatrix}_{aero} = [m_{aero,j}^*] \begin{Bmatrix} \ddot{y}_j \\ \ddot{z}_j \\ \ddot{\theta}_j \end{Bmatrix} + [c_{aero,j}^*] \begin{Bmatrix} \dot{y}_j \\ \dot{z}_j \\ \dot{\theta}_j \end{Bmatrix} + [k_{aero,j}^*] \begin{Bmatrix} y_j \\ z_j \\ \theta_j \end{Bmatrix} \quad (2)$$

where y_j , z_j and θ_j are respectively the lateral, vertical and torsional displacements of the j -th section, $[m_{aero,j}^*]$, $[c_{aero,j}^*]$ and $[k_{aero,j}^*]$ are the aerodynamic matrices related to the j -th section, expressed, per unit length, as

$$[m_{aero,j}^*] = \frac{1}{2} \rho V_j^2 B \begin{bmatrix} p_{6\frac{\pi B}{2V_j^2}}^* & p_{4\frac{\pi B}{2V_j^2}}^* & 0 \\ h_{6\frac{\pi B}{2V_j^2}}^* & h_{4\frac{\pi B}{2V_j^2}}^* & 0 \\ a_{6\frac{\pi B}{2V_j^2}}^* & a_{4\frac{\pi B}{2V_j^2}}^* & 0 \end{bmatrix} \quad (3a)$$

$$[c_{aero,j}^*] = \frac{1}{2} \rho V_j^2 B \begin{bmatrix} -p_{5\frac{1}{V_j}}^* & -p_{1\frac{1}{V_j}}^* & -p_{2\frac{B}{V_j}}^* \\ -h_{5\frac{1}{V_j}}^* & -h_{1\frac{1}{V_j}}^* & -h_{2\frac{B}{V_j}}^* \\ -a_{5\frac{B}{V_j}}^* & -a_{1\frac{B}{V_j}}^* & -a_{2\frac{B^2}{V_j}}^* \end{bmatrix} \quad (3b)$$

$$[k_{aero,j}^*] = \frac{1}{2} \rho V_j^2 B \begin{bmatrix} 0 & 0 & p_3^* \\ 0 & 0 & h_3^* \\ 0 & 0 & a_3^* B \end{bmatrix} \quad (3c)$$

V_j being the mean wind speed for the j -th section, B the bridge deck chord (used as a reference length), and a_i^* , h_i^* and p_i^* with $i = \{1-6\}$ being the flutter derivative coefficients. a_i^* , h_i^* and p_i^* are functions of both the reduced velocity ($V_j^* = V_j/(fB)$, f being the motion frequency), and the angle of attack η_j , that is the function of the mean wind speed itself, being related to the deflected position reached under the mean wind speed stationary load. The mean wind speed V_j is different for each section depending on the elevation of the section itself above the sea level (h_j) in the boundary layer wind profile defined at the considered reference wind speed V . Examples of flutter derivatives of the deck of the Messina Straits Bridge are shown in Fig. 3 for three different angles of attack.

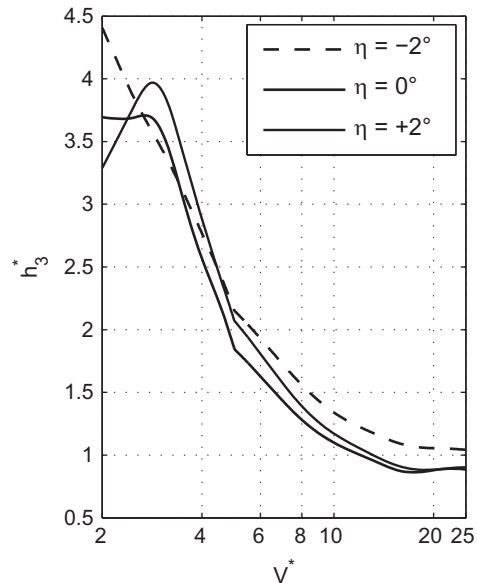


Fig. 3. Example of a_2^* and h_3^* flutter derivatives of the Messina deck section as a function of reduced velocity V^* for different angles of attack.

The definition of the aeroelastic forces (Eqs. (2) and (3)) implies the validity of two hypotheses, considering that the unsteady force coefficients are measured with steady-state forced motion tests:

1. The flutter derivative coefficients, that are measured in steady-state conditions, are assumed to be valid not only for the steady state response of the bridge, but also for the transient response (such as the instability onset).
2. During steady-state forced motion tests, it is not possible to separate the contributions of displacements and relative accelerations to the aeroelastic forces, since they are in-phase (e.g. if $\theta(t) = A \sin(\omega t)$, then $\ddot{\theta}(t) = -\omega^2 A \sin(\omega t)$). Therefore the distinction in aerodynamic mass and stiffness terms reported in Eqs. (3) is done arbitrarily, supported by
 - (a) the idea that the vertical or horizontal variation of position of the deck section does not have any effect in terms of aerodynamic forces (rigorously verified at high V^* , i.e. in the quasi-steady aerodynamics region);
 - (b) the experimental evidence obtained by mutual numerical vs. experimental validation of the implemented code on simple sectional model tests (Diana et al., 2013a).

The motion of the j -th section, which appears in Eq. (2), can be represented using the modal coordinates as

$$\begin{Bmatrix} y_j \\ z_j \\ \theta_j \end{Bmatrix} = [\phi_j] \underline{q} = \phi_{1j} q_1 + \dots + \phi_{Nj} q_N$$

$$= \begin{Bmatrix} y_{1j} \\ z_{1j} \\ \theta_{1j} \end{Bmatrix} + \dots + \begin{Bmatrix} y_{ij} \\ z_{ij} \\ \theta_{ij} \end{Bmatrix} + \dots + \begin{Bmatrix} y_{Nj} \\ z_{Nj} \\ \theta_{Nj} \end{Bmatrix} \quad (4)$$

$[\phi_j]$ being the structural eigenvectors matrix limited to the j -th section: $[\phi_{1j} \dots \phi_{Nj}]$ with N being equal to the total number of modes considered in the model.

The self-excited aeroelastic forces should be calculated assembling the aerodynamic matrices (Eqs. (3)) of the j -th section considering the contribution of each mode, using the flutter derivatives evaluated at the reduced velocity of each i -th mode defined as

$$V_{ij}^* = \frac{V_j}{f_i B} \quad (5)$$

where f_i is the frequency of the i -th mode (being $\omega_i = 2\pi f_i$). The frequency f_i is itself the function of the velocity, and so the problem must be iteratively solved, as it is explained in the next paragraph. Thus, the self-excited aerodynamic drag, lift and moment on the j -th section can be computed as the sum of the considered N modes in the model:

$$\begin{Bmatrix} D_j \\ L_j \\ M_j \end{Bmatrix}_{aero} = \sum_{i=1}^N \left([m_{aero,ij}^*] \begin{Bmatrix} \ddot{y}_{ij} \\ \ddot{z}_{ij} \\ \ddot{\theta}_{ij} \end{Bmatrix} + [c_{aero,ij}^*] \begin{Bmatrix} \dot{y}_{ij} \\ \dot{z}_{ij} \\ \dot{\theta}_{ij} \end{Bmatrix} + [k_{aero,ij}^*] \begin{Bmatrix} y_{ij} \\ z_{ij} \\ \theta_{ij} \end{Bmatrix} \right) \quad (6)$$

where each aerodynamic matrix is a function of V_{ij}^* .

2.2. Iterative non-linear multi-modal eigenvalue algorithm

Using this formulation, combining Eqs. (1) and (6) and summing up the contribution of each section, the modal equations of the coupled aeroelastic system become

$$[M_s^*] \ddot{\underline{q}} + [C_s^*] \dot{\underline{q}} + [K_s^*] \underline{q} = -[M_{aero}^*] \ddot{\underline{q}} - [C_{aero}^*] \dot{\underline{q}} - [K_{aero}^*] \underline{q} \quad (7)$$

$$[M_{s+aero}^*] \ddot{\underline{q}} + [C_{s+aero}^*] \dot{\underline{q}} + [K_{s+aero}^*] \underline{q} = 0 \quad (8)$$

To evaluate the stability of the aeroelastic coupled system defined in Eq. (8), a generalized eigenvalue analysis is performed. Setting the free response of the system as

$$\underline{q} = [\underline{\Xi}] e^{\lambda t} \quad (9)$$

the generalized eigenvalue-eigenvector problem becomes

$$([M_{s+aero}^*(\omega)] \lambda^2 + [C_{s+aero}^*(\omega)] \lambda + [K_{s+aero}^*(\omega)]) [\underline{\Xi}] = 0 \quad (10)$$

The solution of the problem gives the complete set of complex eigenvalues $\lambda = \alpha + j\omega$ and eigenvectors $[\underline{\Xi}]$ of the modal aeroelastic system defined in Eq. (8) as a function of the reference mean wind speed V ($j = \sqrt{-1}$). Therefore for each V it is possible to compute $2N$ of eigensolutions (complex conjugates in pairs):

$$\lambda_i(V) = \alpha_i + j\omega_i \Leftrightarrow \underline{\Xi}_i(V), \quad i = 1, \dots, 2N \quad (11)$$

The eigenvectors $\underline{\Xi}_i$, which are in general complex, express the free motion of the system as a complex linear combination of the structural modes ϕ_i , as follows by combining Eqs. (4) and (9) for a given wind speed. In still air, $[\underline{\Xi}]$ is the identity matrix, because the structural modes are completely uncoupled. Increasing the mean wind speed, this matrix changes, describing the progressive aeroelastic coupling between structural bridge modes.

The peculiarity of this eigenvalue problem is the mutual interdependence between the aeroelastic effects and the eigen-properties of the system. In fact, given a mean wind speed, the aeroelastic matrices (Eq. (8)) are a function of the reduced velocity V^* that (Eq. (5)) depends on the eigenvalues of the system, which are unknown (Eq. (10)).

Due to this nonlinear dependence, the numerical algorithm is made of two main loops. Fig. 4 shows a flowchart that summarizes the whole procedure. The first one updates the mean speed value and through an iterative nonlinear algorithm, it computes the stationary equilibrium position of the structure forced by the mean wind loads. The second loop computes the eigenvalue solution of the aeroelastic system, giving as a result the frequencies and the damping of each mode, at the current mean wind speed. This iterative procedure ends when the difference between the old and the new set of eigenvalues is below a prefixed threshold.

2.3. Monte Carlo simulations

As described in the previous section, the solution of the aeroelastic problem involves many parameters, it is strongly nonlinear, and it has to be iteratively solved. A common procedure that is used to investigate such complex systems is the Monte Carlo simulation technique (MC) (Zio and Marseguerra, 2002; Baraldi et al., 2010).

Considering a problem in which a variable δ is a function of n independent variables β_j (i.e. $\delta = \delta(\beta_1, \dots, \beta_n)$), it is possible that a closed-form solution linking the uncertainties of the inputs to the distribution of the output does not exist. A numerical method to solve this problem is the MC method that requires the knowledge of the statistical distributions of the n independent variables to numerically obtain the distribution of the dependent variable δ .

The number of simulations performed is equal to the number of the iso-probability bands in which the distributions of the independent variables are divided, in order to sample the corresponding realizations of δ . The greater is the number of simulations, the greater is the statistical reliability of the results. We call the number of simulations *sample size* (SS). If SS were equal to infinity, we would have the perfect description of the dependent variable distribution; in practice, we have to check that the statistical dispersion of the MC output data is stable over a threshold of SS.

Given the sample size SS and the number of independent variables n , the MC method allows one to select the values of the x_j for each simulation through the so-called *Monte Carlo Matrix*

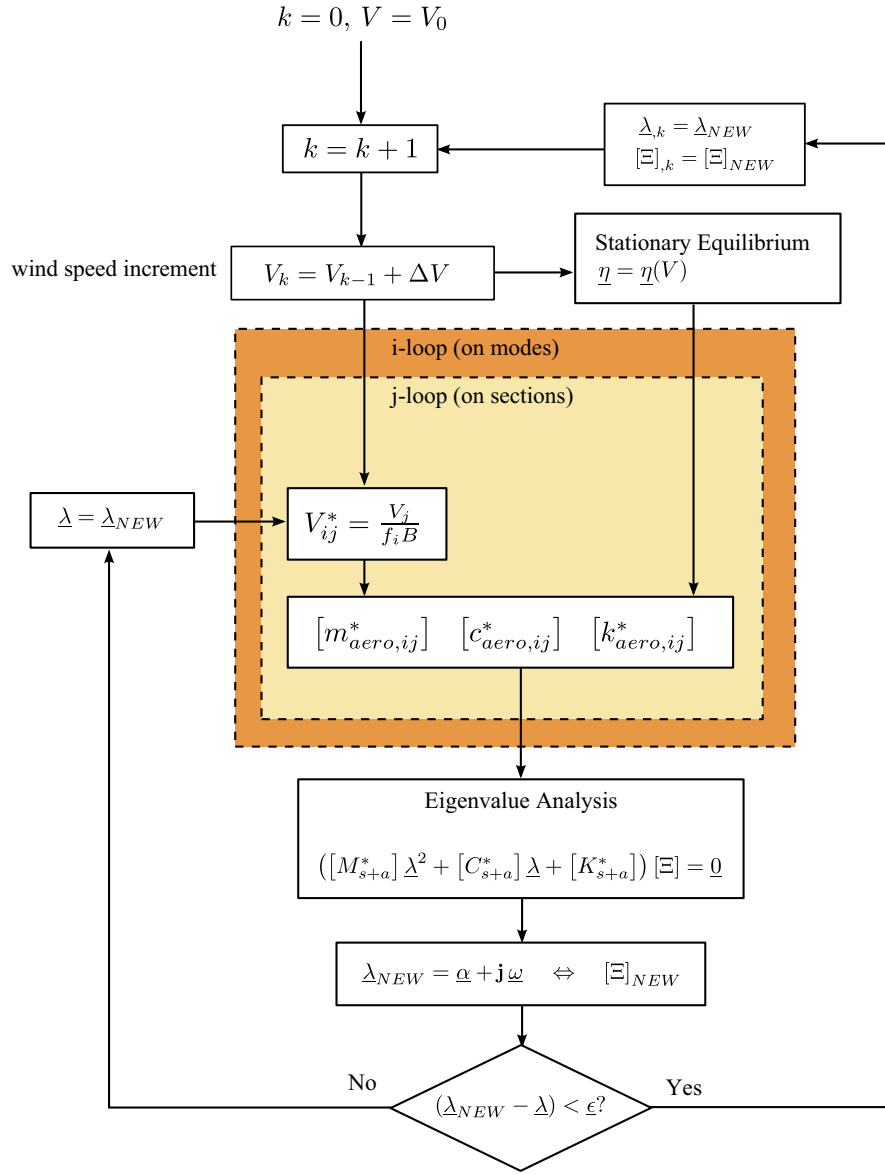


Fig. 4. Flowchart: iterative eigenvalue analysis procedure.

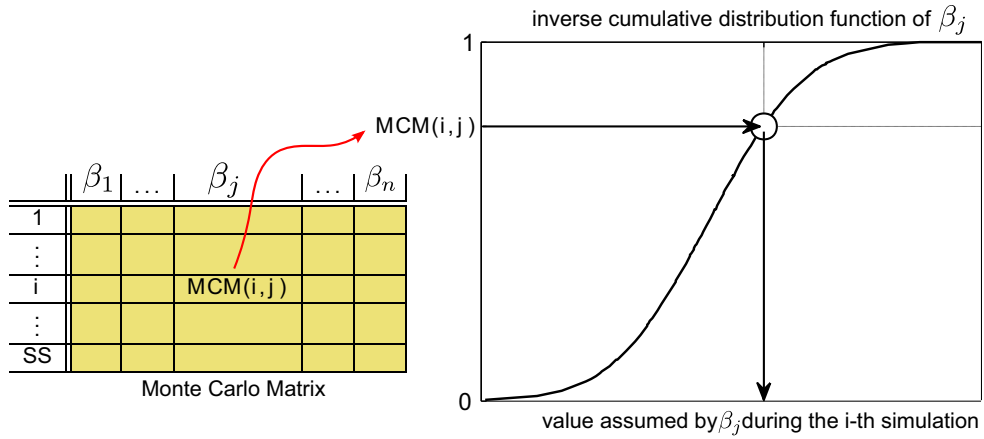


Fig. 5. MC matrix and inverse cumulative probability function of the variable β_j during i -th simulation.

(MCM). Each element of the MCM is a random number uniformly distributed between 0 and 1, and it corresponds to the inverse cumulative probability which the variable β_i assumes during the i -th simulation, as sketched in Fig. 5.

2.4. Uncertainties considered in the analysis

Dealing with aerodynamic stability, wind and structural engineers has to manage with two main kinds of uncertainties:

- uncertainties about the structural properties of the bridge;
- uncertainties about the aerodynamic characteristics of the deck section.

The first kind of uncertainties concerns the structural properties of the bridge, both mechanical and geometrical. Starting from

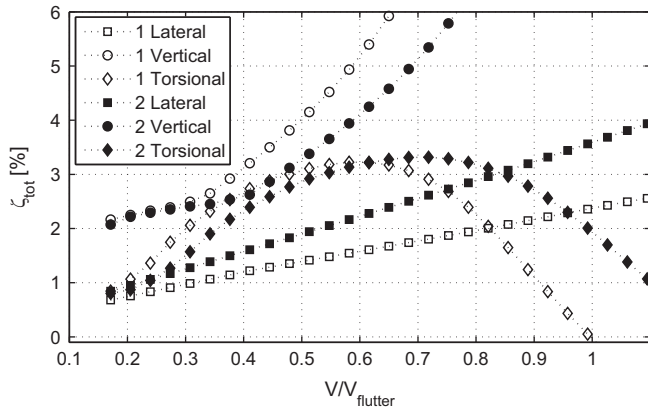


Fig. 6. Multi modal analysis (150 modes) – for clarity we report only the trend of first and second lateral, vertical and torsional deck modes.

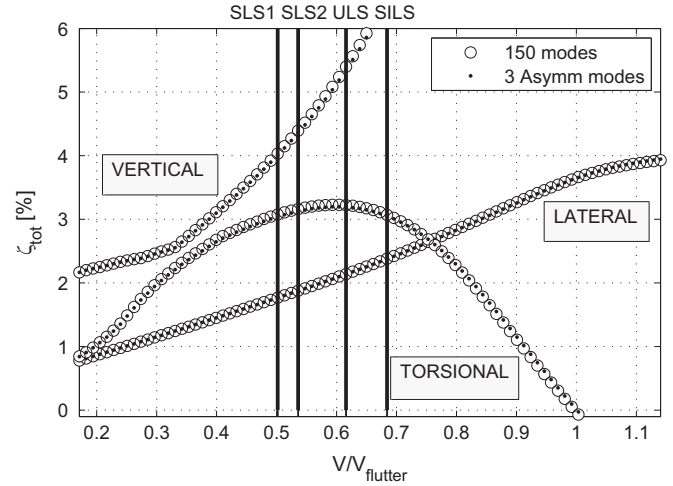
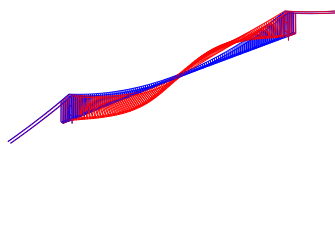
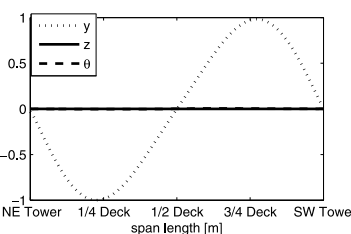
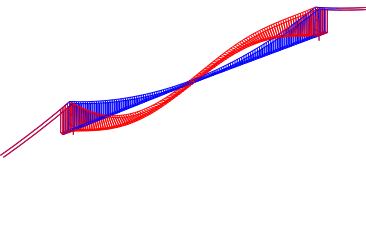
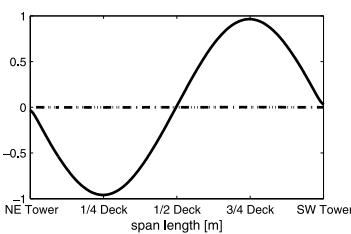
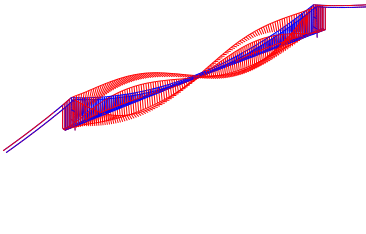
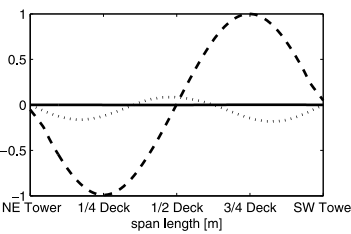


Fig. 7. Comparison between flutter analysis with all modes and only first asymmetric ones - nominal parameters (both structural and aerodynamic).

Table 1

Main properties of the first asymmetrical modes: modal shapes, frequency ratios, and modal mass ratios.

Mode	Isometric view		$\frac{\omega_\theta}{\omega}$	$\frac{m_\theta}{m}$
lateral (y)			1.45	1.22
vertical (z)			1.23	0.64
torsional (θ)			1	1

the final design of the bridge, a different global and/or local geometrical or technological realization of the project may have an impact on the aeroelastic behavior of the structure, affecting directly mass, frequencies and structural damping of the bridge. A possible estimation of the effect of the variation of these parameters on the bridge structural characteristics may be inferred from the mathematical model of the bridge (typically a FE model) that is used during its design: uncertainty may be related to the correct representativeness of the full scale structure, and to a possible variability of its structural characteristics (e.g. the constraints definitions).

The second kind of uncertainties deals with fluid–structure interaction and with several aerodynamic issues. On the one hand, the analytical models adopted to compute the aerodynamic forces acting on the bridge, approximate the aerodynamic phenomena; on the other hand, they rely on experimental coefficients that are measured in wind tunnel on scaled models. Concerning the experimental coefficients, apart from uncertainties related to the

measurement process, other sources of uncertainty are the wind tunnel flow and the model characteristics: Reynolds number self-similarity, the residual turbulence of nominal smooth flow, the surface roughness of the model, the appropriate representation of the aerodynamic effects of sharp edges, and so on.

From an engineering point of view, all these uncertainties have to be carefully taken into account in the evaluation of the aeroelastic stability since they have a great effect on the results. This is particularly important for very long span bridges, like the one that is considered in this paper, since the design of such a bridge relies on structural and aerodynamic optimizations. In particular, for the Messina Bridge, the deck must be light enough to allow for the railway traffic and characterized by small aerodynamic coefficients to guarantee the aeroelastic stability.

3. Results

In this section we apply the methodology described to the Messina Straits Bridge. It is a suspended bridge with a main span length of 3300 m and a deck chord width of 60 m. The deck has a

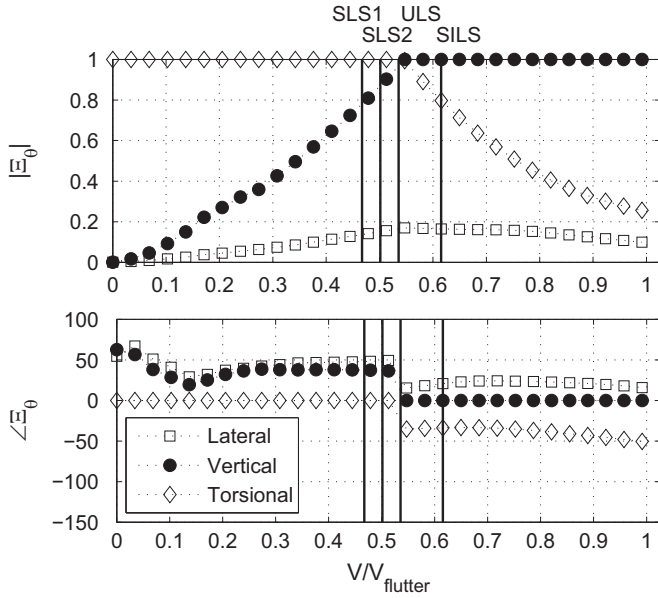


Fig. 8. Evolution of first structural torsional asymmetric mode vs. dimensionless mean wind speed.

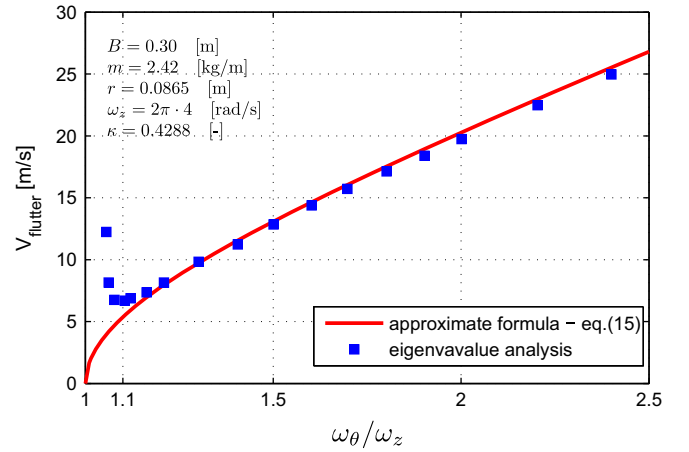


Fig. 10. Flutter velocity as a function of frequency ratio ω_θ/ω_z for a given value of ω_θ (after Matsumoto et al., 2010, Fig. 5).

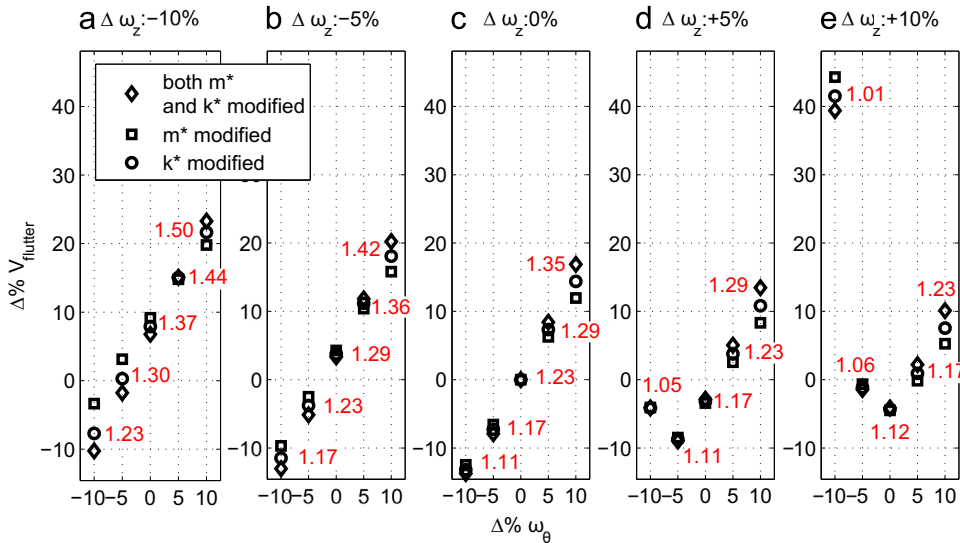


Fig. 9. Flutter velocities for different frequencies variation strategies. Numbers next to markers are the values of the corresponding value of ω_θ/ω_z .

multi-box section, with a central railway girder and two external roadway girders (see Fig. 2).

The numerical results are presented according to the following logic:

1. A stability analysis is performed using nominal input values, and the results are taken as a reference. Besides, this analysis allows one to select the structural modes that are more critical for aerodynamic stability.
2. The aerodynamic and structural input parameters that mostly influence the stability index are selected by means of a deterministic sensitivity analysis.
3. A MC simulation is performed to assess the distribution of the stability index around the nominal value, using the structural modes identified in the first analysis, and taking as

Table 2

Effect on critical flutter velocity and on the total damping of the single and combined variations of vertical and torsional frequencies. Bold rows refer to cases cited in the text.

Input		Output				
$\Delta\%$		$\Delta\%\zeta_{tot}$				$\Delta\%$
ω_z	ω_θ	SLS1	SLS2	ULS	SILS	V_{fl}
-10	-10	-2	-3	-6	-11	-10.2
-10	-5	7	8	11	16	-1.8
-10	0	12	14	20	31	6.8
-10	5	15	17	26	40	15.1
-10	10	17	20	31	46	23.3
-5	-10	-15	-18	-29	-41	-13
-5	-5	-1	-1	-3	-5	-5
-5	0	7	8	12	18	3.4
-5	5	11	14	21	32	11.9
-5	10	14	17	26	40	20.3
0	-10	-38	-44	-59	-70	-13.7
0	-5	-13	-15	-23	-33	-7.9
0	5	7	8	13	20	8.4
0	10	11	13	21	33	16.9
5	-10	-66	-71	-79	-83	-4.1
5	-5	-33	-38	-51	-62	-8.9
5	0	1	1	2	4	-2.8
5	5	-11	-13	-19	-26	5.1
5	10	7	8	14	22	13.5
10	-10	-77	-78	-80	-80	39.4
10	-5	-60	-65	-74	-79	-1.4
10	0	-28	-33	-44	-55	-4.1
10	5	-9	-10	-15	-20	2.2
10	10	1	1	4	7	10.1

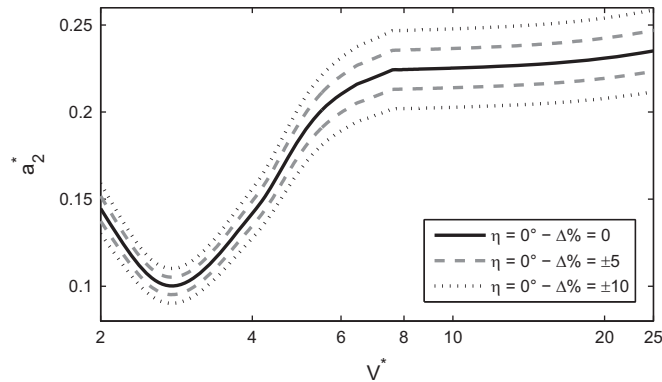


Fig. 11. Example of flutter derivative coefficient with the considered ranges of variation.

independent variables the parameters selected in the second one. A Gaussian distribution is assumed for all the input parameters, with variances that are in the range of those reported by other researchers (e.g. Cheng et al., 2005).

3.1. Deterministic approach using nominal values

The first analysis was performed considering the nominal values of both structural and aerodynamic parameters. In particular, each modal dimensionless damping ratio ζ_{str} is assumed

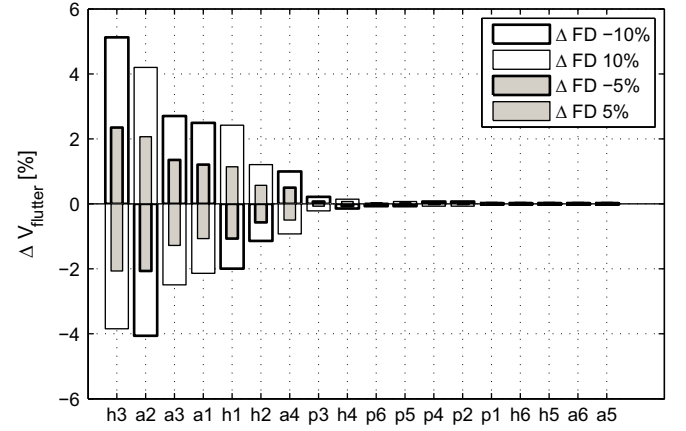


Fig. 12. Influence of single flutter derivatives on flutter speed variation.

Table 3

Effect on total damping of the single variations of most significant Flutter derivatives.

	$\Delta\%FD$	$\Delta\%\zeta_{tot}$				$\Delta\%V_{fl}$
		SLS1	SLS2	ULS	SILS	
a_2^*	-10	-12	-13	-14	-16	-4.1
	-5	-6	-6	-7	-8	-2.1
	5	6	6	7	8	2.1
	10	12	13	14	17	4.2
h_3^*	-10	2	3	5	7	5.1
	-5	1	1	2	3	2.3
	5	-1	-1	-2	-3	-2.1
	10	-2	-3	-5	-7	-3.8
a_1^*	-10	2	3	4	6	2.5
	-5	1	1	2	3	1.2
	5	-1	-1	-2	-3	-1.1
	10	-2	-3	-4	-6	-2.1
a_4^*	-10	0.9	1.0	1.3	1.8	1
	-5	0.5	0.5	0.6	0.9	0.5
	5	-0.5	-0.5	-0.7	-0.9	-0.5
	10	-0.9	-1.0	-1.3	-1.8	-0.9
h_2^*	-10	0.8	0.8	0.8	0.6	-1.1
	-5	0.4	0.4	0.4	0.3	-0.6
	5	-0.4	-0.4	-0.4	-0.3	0.6
	10	-0.8	-0.8	-0.8	-0.6	1.2
h_1^*	-10	-0.1	-0.1	-0.3	-0.7	-2
	-5	-0.1	-0.1	-0.2	-0.4	-1.1
	5	0.1	0.1	0.2	0.4	1.1
	10	0.1	0.2	0.4	0.8	2.4
a_3^*	10	> -0.1				-2.5
	-5					-1.3
	10	< 0.1				1.4
	-5					2.7

equal to 0.3%. Results are reported in terms of total damping coefficient ζ_{tot} , which is taken as a stability index.

For each mode, the stability index is defined as

$$\zeta_{tot} = -\alpha/|\lambda| \quad (12)$$

where α is the real part of the eigenvalue λ and $|\lambda|$ its magnitude.

The total damping is computed at different values of mean wind speed corresponding to prescribed return periods reported in the Messina Strait Bridge technical requirements as SLS1, SLS2, ULS and SILS (associated to a return period of 50, 200, 2000 and greater than 2000 years).

The stability analysis was initially performed using the first 150 structural modes. The analysis (150 modes – Fig. 6) allows one to understand the flutter phenomenon of the Messina suspension bridge. The aerodynamic instability occurs due to the coupling of the first vertical and torsional asymmetric deck modes. It is worthy to underline that this behavior is exhibited by all the vertical-torsional homologous couples of modes (higher than the first), but the instability occurs at higher wind speeds. Moreover it is important to note that only the torsional modes are negatively affected by aerodynamics, since the total damping of lateral and vertical bending modes always increases with wind speed. In the following, we will focus our attention only onto the index of stability of this mode.

A second stability analysis was performed considering the first three modes involved in flutter coupling (first lateral bending, vertical bending and torsional asymmetric modes) whose properties are reported in Table 1.

Using only the first asymmetric set of modes instead of the larger initial modal base (3 modes vs. 150 modes – Fig. 7), the numerical procedure still allows one to perform a very accurate prevision of the influence of the mean wind speed onto the damping of the modes (the error is less than 1%), and therefore only the first three modes will be considered in the following. This result is consistent with previous studies about flutter of bridges (e.g. Chen et al., 2000, 2001).

The evolution of the torsional mode shape, as a function of the wind speed, is shown in Fig. 8. This mode gradually couples with the vertical one, and at flutter speed the torsional motion has with a phase lead of 130° with respect to the vertical one. At instability, in physical coordinates, the displacement of the quarter-span section at the leading edge will be

$$z_{edge} = z + \theta \frac{B}{2} = 1 \cdot \sin(\omega t) + 0.26 \cdot \sin(\omega t - 50^\circ) \quad (13)$$

3.2. Deterministic sensitivity analysis

The sensitivity analysis is performed to evaluate the influence of both mechanical and aerodynamic parameters on the stability index, and to focus the attention onto the most significant ones. The parameters considered in the deterministic stability analysis are the structural parameters of the involved modes (modal mass and stiffness) and the aerodynamic coefficients (p_i^* , h_i^* and a_i^*).

Table 4

MC simulations: summary of tested uncertainties combinations. The elements in the cells are the SS tested.

	$\Delta\% \omega$		
	± 5	± 10	± 15
$\Delta\% FD$			
± 5	50, 100, 150, 500, 1000	50, 100, 150, 500, 1000	50, 100, 150, 500, 1000
± 10	50, 100, 150, 500, 1000	50, 100, 150, 500, 1000, 2500, 5000	750, 10 000
± 15	50, 100, 150, 500, 1000		
± 20	50, 100, 150, 500, 1000, 2500, 5000		

3.2.1. Modal parameters

First, the effects of a change in the structural frequencies were analyzed; this analysis allows one to indirectly consider structural nonlinearities, such as the change in stiffness due to static aerodynamic stresses. It is worth noting that to obtain a given variation of the circular frequency, several strategies are available. In fact, γ being the variation factor, to modify the frequency from ω to $\hat{\omega} = \gamma\omega$ we have to manage the variation of modal mass and stiffness parameters (m and k):

$$\hat{\omega} = \gamma\omega = \gamma\sqrt{\frac{k}{m}} = \sqrt{\frac{\hat{k}}{\hat{m}}} \quad (14)$$

Since it is not clear from experimental campaigns, based on output-only identification methods (e.g. Qin et al., 2001; Çevik and Pakdemirli, 2005), whether uncertainties in eigen-frequencies of long span bridges are due to uncertainties in either mass or stiffness, three different variation strategies have been investigated:

- Variation of frequency due to a mass change only: $\hat{m} = m/\gamma^2$ and $\hat{k} = k$.
- Variation of frequency due to a stiffness change only: $\hat{m} = m$ and $\hat{k} = k\gamma^2$.
- Variation of frequency due to an equal variation in stiffness and mass: $\hat{m} = m/\gamma$ and $\hat{k} = k\gamma$.

To compare these three methods, we performed some tests using all the possible combinations of both the variations of the vertical (ω_z) and torsional (ω_θ) frequencies equal to -10% , -5% , $+5\%$, $+10\%$.

The variation of the lateral frequency has negligible effects and it is not discussed in the rest of the paper. Finally, we highlight that when the modal mass or stiffness changes, the corresponding modal shape is not modified.

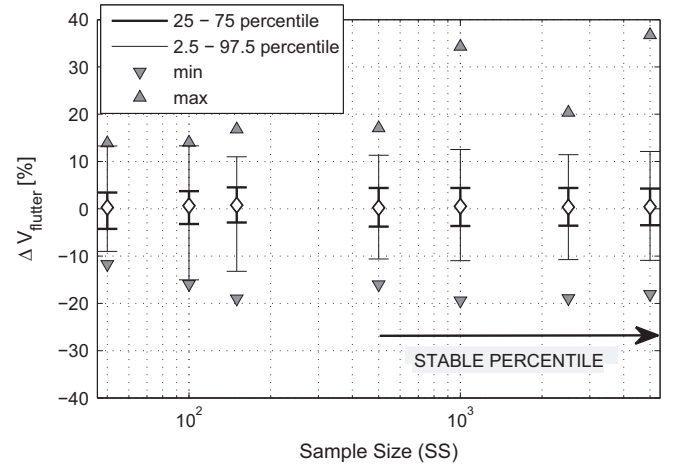


Fig. 13. Statistical analysis of results increasing SS ($\Delta\% \omega = \Delta\% FD = \pm 10\%$). Thin line: 2.5–97.5% percentiles, bold line: 25–75% percentiles.

In the following, any variation of a given parameter ξ is defined as a percentage of variation with respect to its nominal value, and identified with the nomenclature $\Delta\%\xi$.

Results for flutter velocity are reported in Fig. 9. Two parameters mainly influence the flutter speed: the frequency ratio ω_θ/ω_z and the torsional frequency ω_θ . As it has been reported in previous studies (Dyrbye and Hansen, 1997; Matsumoto et al., 2010), flutter speed has a minimum for $\omega_\theta/\omega_z \approx 1.1$. Moreover, for frequency ratios higher than that threshold, the Selberg formula, or other approximate analytical formulas (Chen, 2007; Matsumoto et al., 2010), can be used to analyze the flutter critical speed (see Fig. 10).

For the case $\omega_\theta/\omega_z > 1.1$ the simplified formula of Chen (2007) can be used. This formula states

$$V_{flutter} = \kappa \omega_\theta b \sqrt{\left(1 - \frac{\omega_z^2}{\omega_\theta^2}\right) \left(\frac{mr}{\rho b^3}\right)} \quad (15)$$

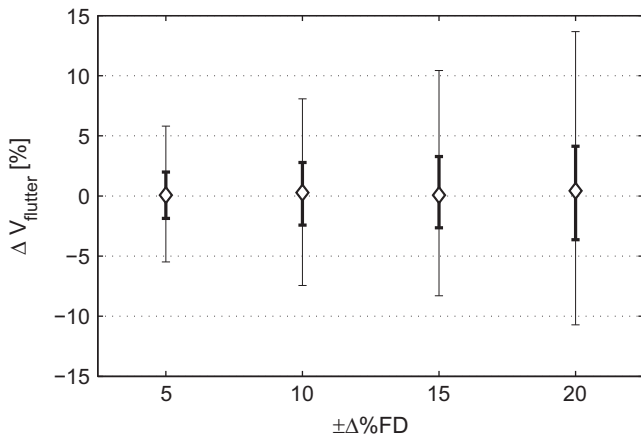


Fig. 14. MC results: variation of critical flutter speed and total damping percentiles obtained increasing FD variations range with $\Delta\%\omega = \pm 5$. Thin line: 2.5–97.5% percentiles, bold line: 25–75% percentiles.

where κ is a parameter that depends non-linearly on flutter derivatives, b is the half-chord length, m and $I = mr^2$ are the effective modal mass and moment of inertia per unit span, respectively. It can be easily seen that the flutter speed is proportional to the torsional frequency and to the frequency ratio ω_θ/ω_z .

Comparing the three methods of varying the frequencies presented in Fig. 9, it can be noticed that they all show the same trend, therefore we decided to proceed in the analysis using the strategy of modifying both modal mass and stiffness, since it leads to the largest percentage variations.

Variations of the frequencies have a remarkable effect, not only on the critical mean wind speed at which flutter occurs, but also on the total damping. Numerical results are reported in detail in Table 2 for all the considered combinations. It is interesting to note that the variation of critical flutter velocity and the variation of the

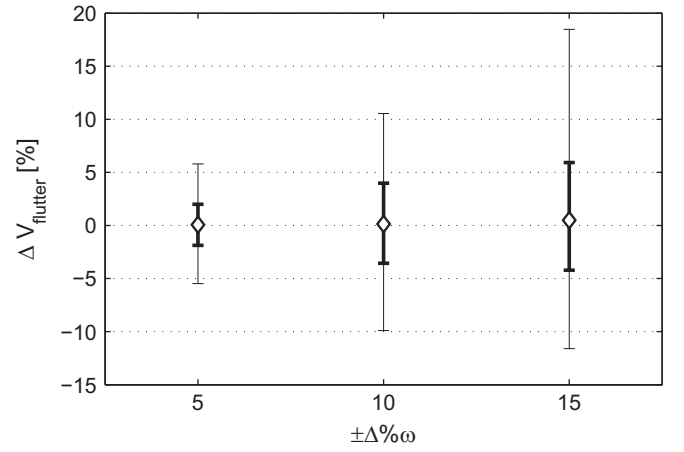


Fig. 16. MC results: variation of critical flutter speed percentile obtained increasing frequencies variations range $\Delta\%FD = \pm 5$. Thin line: 2.5–97.5% percentiles, bold line: 25–75% percentiles.

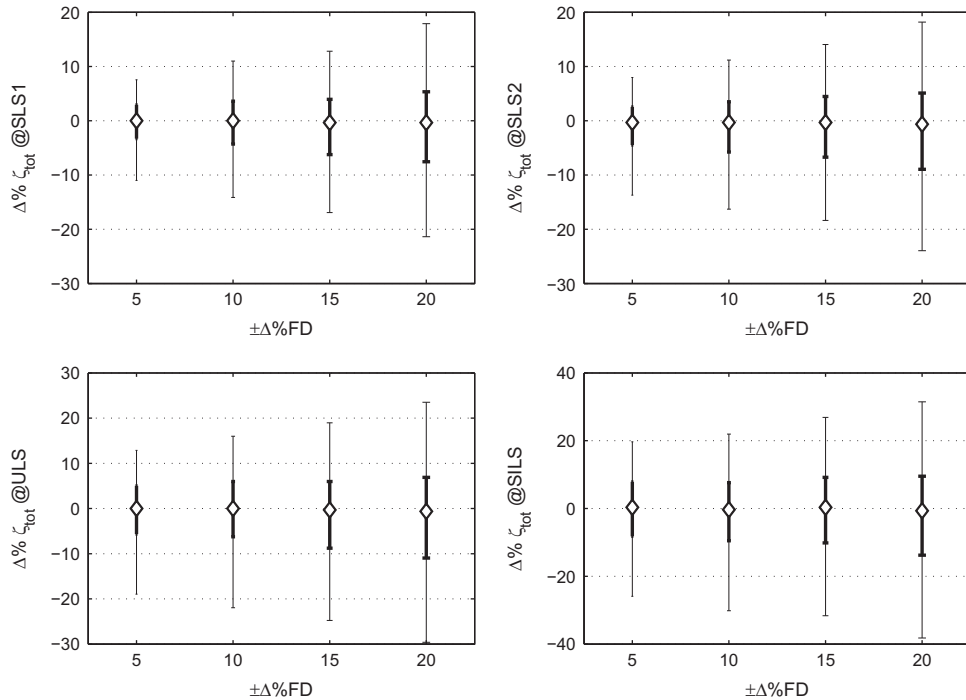


Fig. 15. MC results: variation of total damping percentiles obtained increasing FD variations range $\Delta\%\omega = \pm 5$. Thin line: 2.5–97.5% percentiles, bold line: 25–75% percentiles.

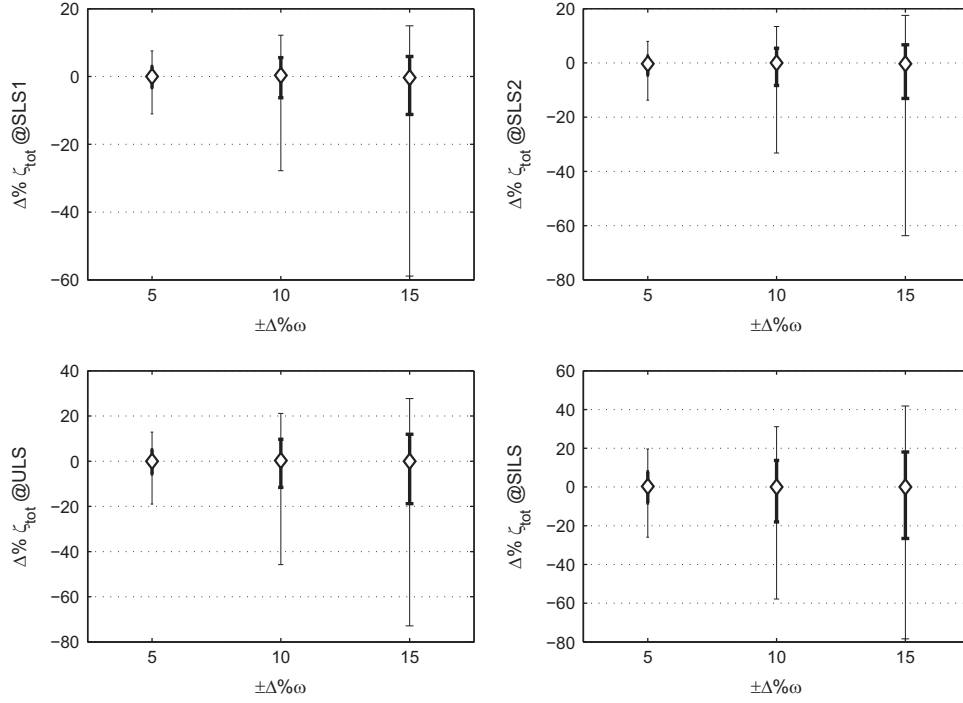


Fig. 17. MC results: variation of total damping percentile at different service states obtained increasing frequencies variations range $\Delta\%FD = \pm 5$. Thin line: 2.5–97.5 percentiles, bold line: 25–75% percentiles.

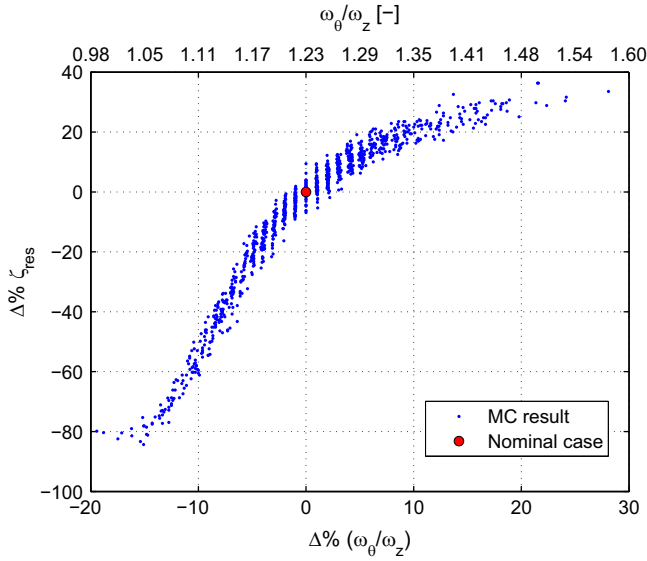


Fig. 18. Variation of ζ_{tot} as a function of the variation of ω_θ/ω_z for the simulation $\Delta\%\omega = \pm 15$ and $\Delta\%FD = \pm 5$ at ULS velocity.

total damping are not correlated. As an example, the combinations $[\Delta\%\omega_z = -10; \Delta\%\omega_\theta = -5]$ and $[\Delta\%\omega_z = -5; \Delta\%\omega_\theta = 0]$ show equal variation of the total damping, but opposite results regarding the critical velocity. The combinations $[\Delta\%\omega_z = 5; \Delta\%\omega_\theta = -10]$ and $[\Delta\%\omega_z = 10; \Delta\%\omega_\theta = 0]$ have a similar flutter wind speed variation, but a different one for damping.

3.2.2. Aerodynamic coefficients

Dealing with the aerodynamic parameters, an analysis similar to the previous one has been done in order to establish which are the flutter derivatives that mainly influence the stability of the structure. Four levels of variation for each flutter derivatives were

tested ($\pm 10\%$ and $\pm 5\%$), fixing the remaining parameters to their nominal value. As an example, in Fig. 11 the ranges of variation for the a_2^* coefficient considered in the analysis are reported.

It is shown in Fig. 12 that h_3^* , a_2^* , a_3^* , and a_1^* have the most relevant influence on flutter stability, while the total damping is strongly influenced by a_2^* , with a minor effect of h_3^* and a_1^* (Table 3). The effects of the others flutter derivatives are negligible. These results confirm previous findings, based on simplified analytical and numerical approaches (Matsumoto et al., 1996; Chen, 2007; Matsumoto et al., 2010).

It is important to underline that the influence of the aerodynamic parameters is different if we analyze the critical or the service state wind speeds considering the progressive aeroelastic coupling between modes, as already introduced in Fig. 8. As an example, simplifying the problem, it can be noticed that the variation of the torsional modal total damping, at lower value of mean wind speed where the mode is still a torsional mode, is mainly influenced by a_2^* (equivalent damping effect on the torsional mode due to aerodynamic moment), while, near the critical value of mean wind speed, when the structural-torsional mode has already a relevant vertical component, it is largely influenced by h_3^* , whose effect is to couple the torsional and the vertical motion (cf. Eq. (3c)).

Even if a correlation between some flutter derivatives at high reduced velocity can be found using quasi-steady theory, it is not straightforward to define a correlation model between flutter derivatives in all the reduced velocity range (Scanlan et al., 1997), because many factors are involved (both experimental and theoretical). Therefore these coefficients will be considered uncorrelated random variables.

Last but not least, this analysis let us to select the parameters whose variations produce a negligible effect on stability. Dealing with the modal structural parameters, the modal damping is neglected because it represents only an offset of the stability analysis. On the other hand, the flutter derivatives related to the lateral dynamic motion and to the vertical acceleration, respectively p_i^* (with $i = 1-6$) and h_4^* , could be disregarded.

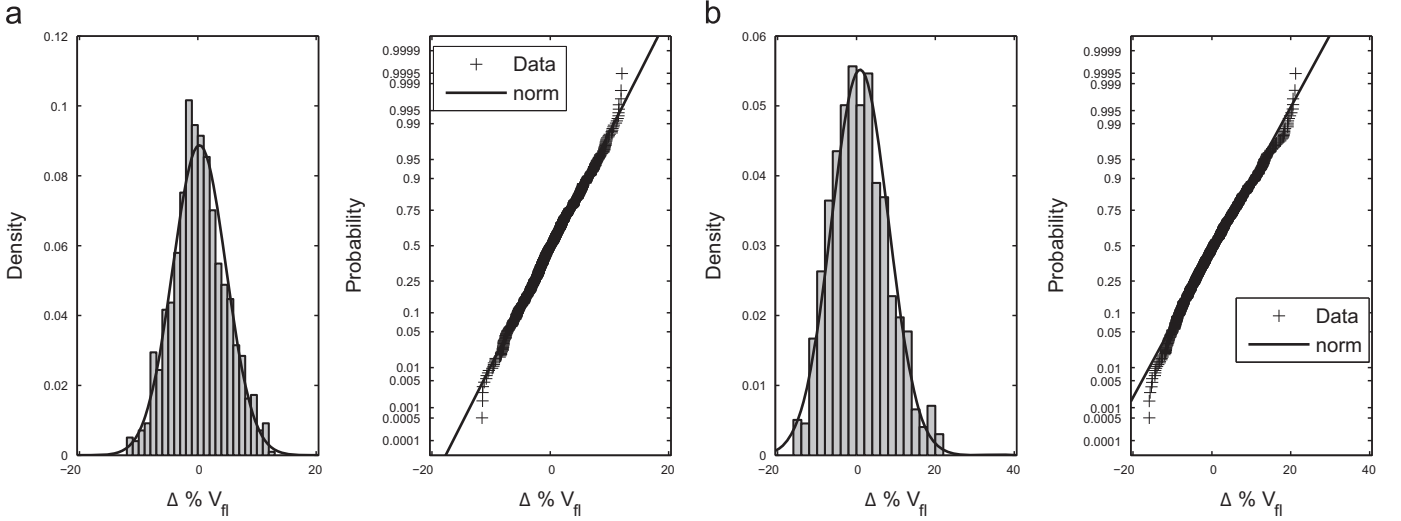


Fig. 19. Flutter speed variation: comparison between MC simulation results and probability fit with $\Delta\%\omega = \pm 5\%$ & $\Delta\%FD = \pm 15\%$ (a) and $\Delta\%\omega = \pm 15\%$ & $\Delta\%FD = \pm 5\%$ (b).

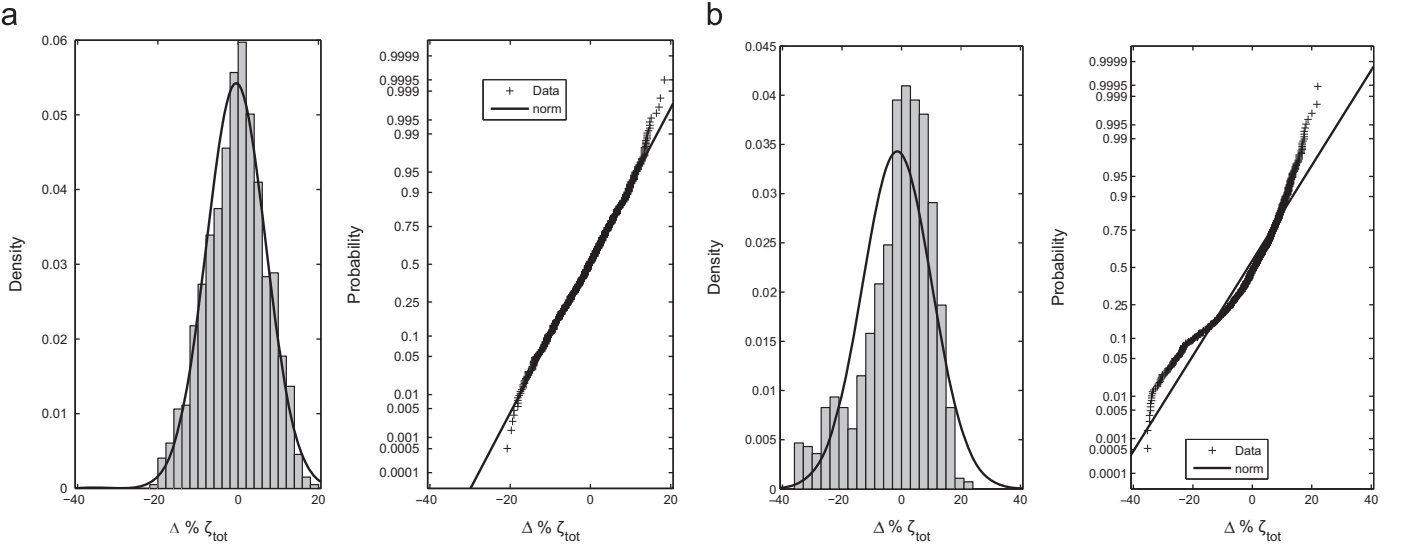


Fig. 20. Total damping coefficients variation at SLS1: comparison between MC simulation results and probability fit with $\Delta\%\omega = \pm 5\%$ & $\Delta\%FD = \pm 15\%$ (a) and $\Delta\%\omega = \pm 15\%$ & $\Delta\%FD = \pm 5\%$ (b).

3.2.3. Summary of sensitivity analysis

Using the previous results, the parameters that will be varied in the statistical analysis will be: both the structural vertical and torsional frequencies (two independent random variables), and the aerodynamic parameters a_i^* with $i=1-4$, and h_i^* with $i=1-3$ (seven independent random variables). Therefore a total of nine random variables will be used in the statistical analysis.

As a final comment, considering a different angle of attack η_i for each deck section produces negligible effects (the maximum rotation of deck section at mid-span is less than 1 deg at SILS and the aerodynamic coefficients have a very small slopes). Thus, in the following analysis, we neglect the stationary deflection of the bridge. Moreover, additional simulations highlighted that towers and cables effect do not significantly influence the results and thus they will be disregarded (Zasso et al., 2013).

3.3. Statistical analysis of critical flutter velocity and total damping trend

To compute a statistical evaluation of the sensitivity of the bridge stability, due to the simultaneous variation of the

above-mentioned parameters, Monte Carlo simulations were performed with different sample sizes (SS) and uncertainty levels.

Each random variable δ is varied as $\delta_{varied} = \epsilon \cdot \delta_{nominal}$. The variation parameter ϵ is described by a *Normal distribution* with the mean value being equal to 1, and setting the standard deviation of the data σ equal to $\Delta\epsilon/3$, so that the probability of having a value of ϵ in the range $\mu - 3\sigma < \epsilon < \mu + 3\sigma$ is equal to 99.73% (i.e. $\int_{\mu-3\sigma}^{\mu+3\sigma} PDF(\epsilon, \mu, \sigma) d\epsilon = 99.73\%$). It is worth noting that the normal distribution is symmetric, but other distributions might be chosen, as an example of a log-normal distribution (e.g. Pourzeynail, 2002; Cheng et al., 2005).

Different combinations of variations of mechanical and aerodynamic parameters were tested as summarized in Table 4, containing sample size for each corresponding combination.

The very first check of the analysis is to verify and set the SS threshold in order to achieve reliable results. Fig. 13 shows the 2.5–97.5 and the 25–75 percentile of results obtained with several $\Delta\%\omega = \Delta\%FD = \pm 10\%$ simulations as a function of an increasing value of SS. It can be seen that, approximately for SS greater than 500, all the values of percentiles are stable, so the SS threshold has been set to 1000. It is clear that the maximum and

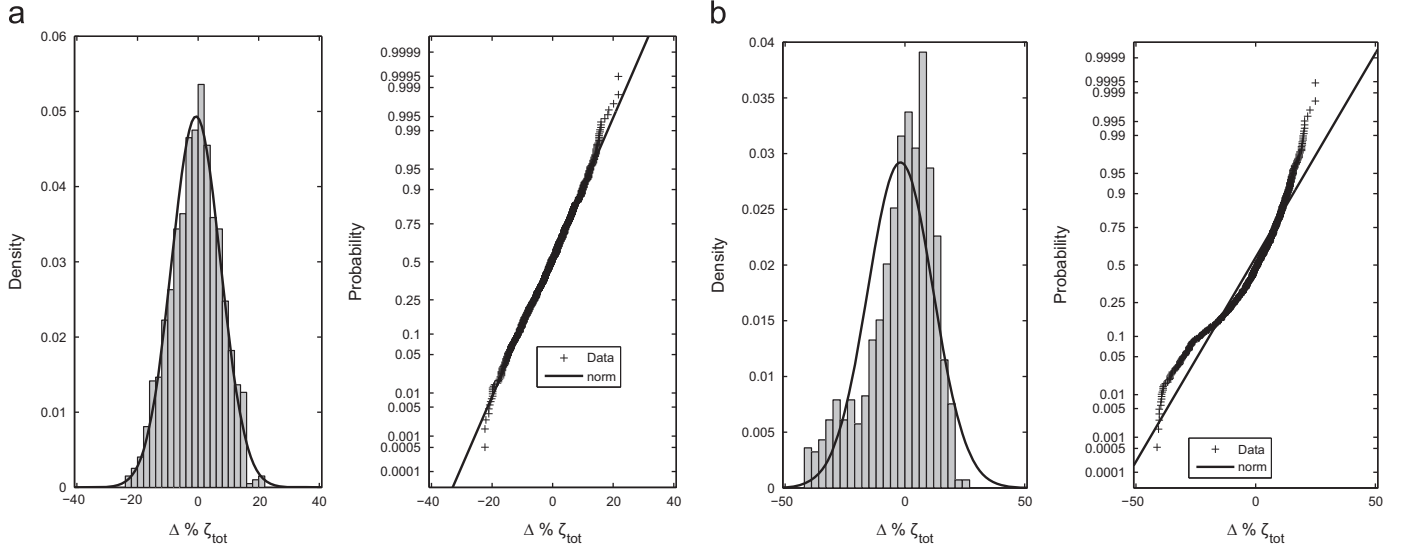


Fig. 21. Total damping coefficients variation at SLS2: comparison between MC simulation results and probability fit with $\Delta \% \omega = \pm 5\%$ & $\Delta \% FD = \pm 15\%$ (a) and $\Delta \% \omega = \pm 15\%$ & $\Delta \% FD = \pm 5\%$ (b).

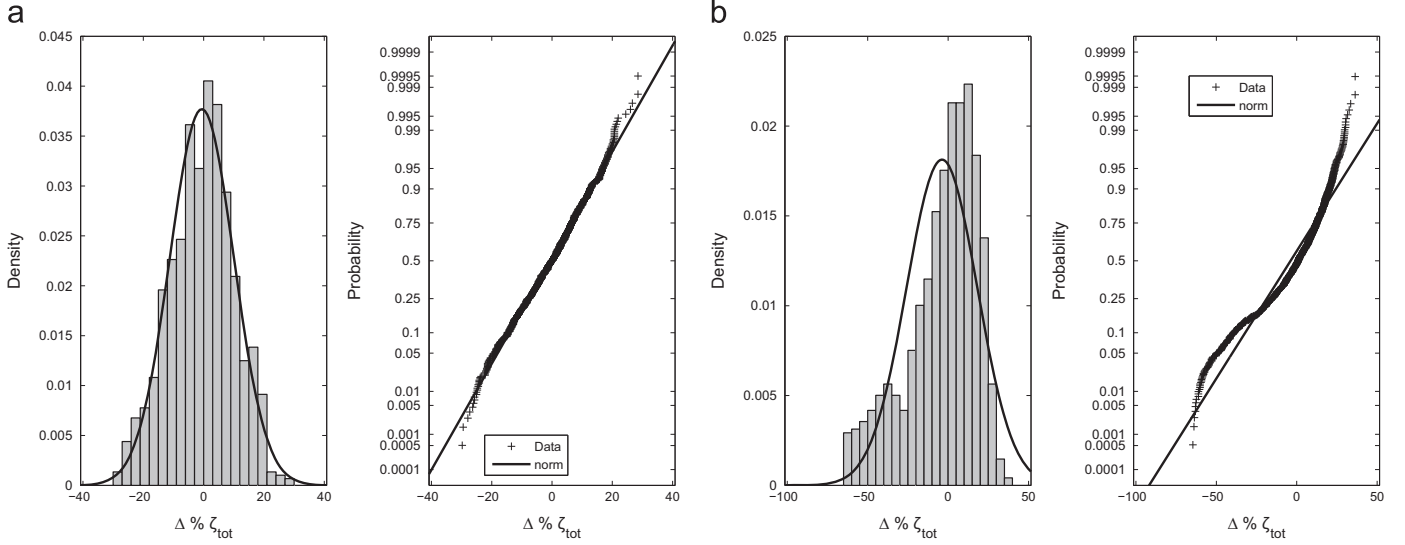


Fig. 22. Total damping coefficients variation at ULS: comparison between MC simulation results and probability fit with $\Delta \% \omega = \pm 5\%$ & $\Delta \% FD = \pm 15\%$ (a) and $\Delta \% \omega = \pm 15\%$ & $\Delta \% FD = \pm 5\%$ (b).

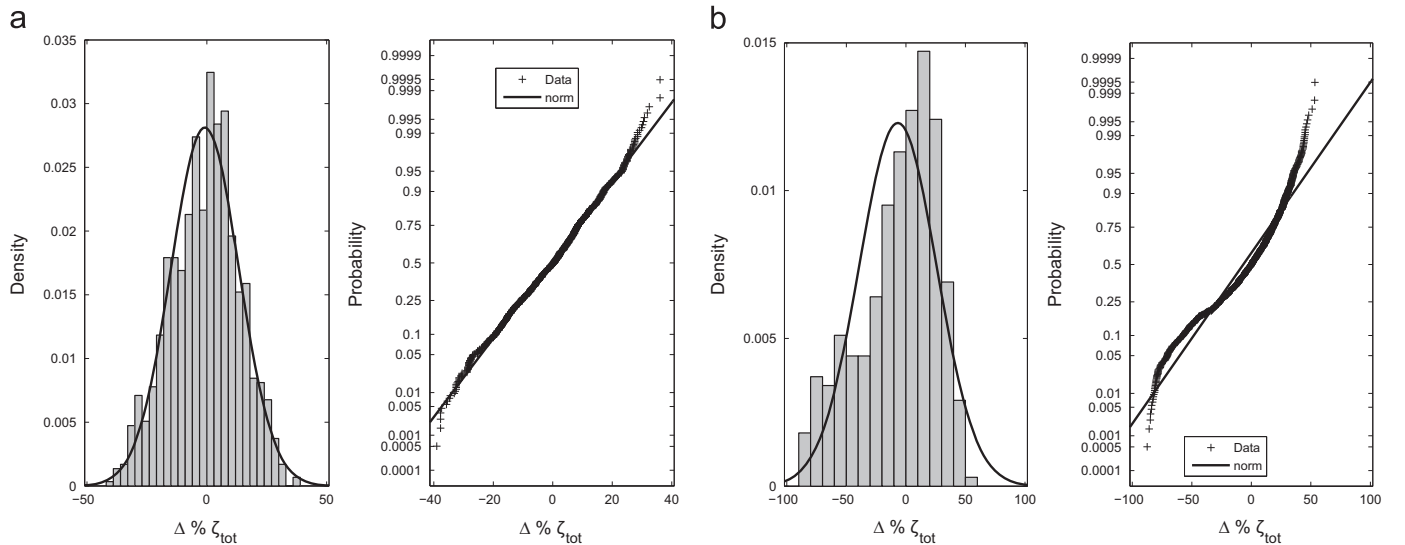


Fig. 23. Total damping coefficients variation at SILS: comparison between MC simulation results and probability fit with $\Delta \% \omega = \pm 5\%$ & $\Delta \% FD = \pm 15\%$ (a) and $\Delta \% \omega = \pm 15\%$ & $\Delta \% FD = \pm 5\%$ (b).

the minimum values do not follow a threshold rule, because, increasing the number of SS, the tails of the input distributions are better evaluated: it is possible that an extreme realization of the dependent variable occurs, even if the scatter of the whole set of simulations is still constant. This does not represent a problem since the single maximum and minimum value are negligible from a statistical point of view.

Several MC simulations were performed fixing the variations of the frequencies $\Delta\omega$ and increasing the scatter of the aerodynamics parameters ΔFD , and vice versa, in order to verify if the results obtained with the MC simulations were similar to those of the deterministic analysis.

Increasing the scatter of the aerodynamic parameters, with a constant frequency variation level, (i.e. $\Delta FD = \pm 5, \pm 10, \pm 15, \pm 20; \Delta\omega = \pm 5$), results regarding both critical flutter velocity and total damping at different service states increase their scatter, as shown in Figs. 14 and 15. These Figures report the median, the 2.5–97.5%, and the 25–75 percentile: it can be noted that the distributions tend to be asymmetric increasing the variations of the aerodynamic parameters.

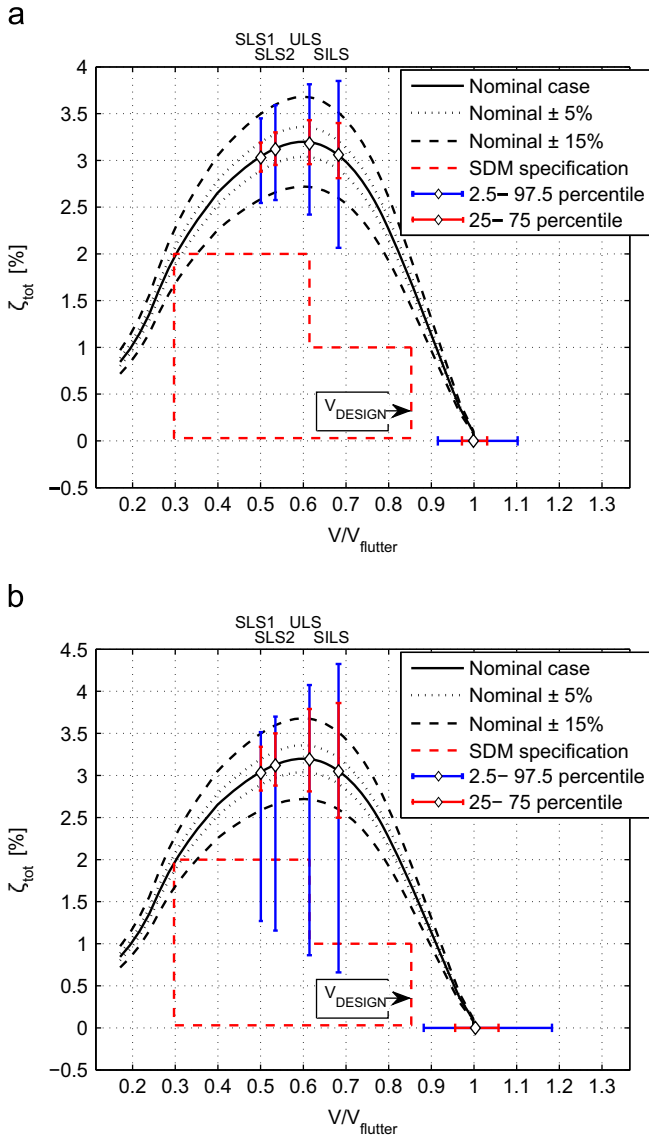


Fig. 24. Total damping and critical velocity statistics: comparison between MC simulation results with $\Delta\omega = \pm 5\%$ & $\Delta FD = \pm 15\%$ (a) and $\Delta\omega = \pm 15\%$ & $\Delta FD = \pm 5\%$ (b).

Considering the frequency variation with a low level of scatter of the aerodynamic coefficients (i.e. $\Delta\omega = \pm 5, \pm 10, \pm 15; \Delta FD = \pm 5$), the scatter of the flutter velocity increases with the growing of the assigned range of variation of the frequencies (Fig. 16): it is not symmetric with larger variation on the positive values. Considering variations of the same order of magnitude, the influence of the modal parameters affects the critical flutter speed more than the aerodynamic coefficients.

Increasing the uncertainty of frequencies, the variation range of the total damping increases, as shown in Fig. 17. The behavior is very asymmetric, as described for the critical flutter velocity, but the asymmetry is larger towards negative variations.

This asymmetry can be explained looking at the dependence of ζ_{tot} on the parameter ω_θ/ω_z . As an example, considering the result at ULS velocity for $\Delta\omega = \pm 15$, reported in Fig. 18, it is possible to notice the nonlinear dependence of the variation of ζ_{tot} on the variation of ω_θ/ω_z , which explains the asymmetric distribution.

It is confirmed that, for the considered bridge, the stability of the structure is more affected by frequency variations than by a change in the aerodynamic parameters (considering the same level of uncertainty). This seems consistent with analytical formulas for total damping (e.g. Chen, 2007; Matsumoto et al., 2010), in which the highly nonlinear dependence on structural frequency is highlighted.

Fitting the data with a probability distribution is the next step of the analysis. A unique distribution to fit the results was not found, mainly due to the asymmetric shape of the tails. As a reference, a fitting using the likelihood method was performed using a *Normal probability distribution*. The goodness of the fitting is directly linked to the magnitude of the variation and to the non-linearity of the results.

As far as the flutter speed is concerned (Fig. 19), the scatter of the results is well fitted by the normal distribution function, both for large variations of the flutter derivatives (19a) and for large variations of the frequencies (19b). On the contrary, analyzing the distributions for the total damping (Figures from 20 to 23), if large variations of flutter derivatives are considered the normal distribution fits quite well the results (20a to 23a), while for large variations of the frequencies the fit is not good, highlighting the highly nonlinear dependence of the total damping on the frequency ratio ω_θ/ω_z .

The analysis performed also allows one to state the probability of not matching the technical specifications, and the probability of being in a certain prescribed variation band. Considering the previous scenarios ($\Delta\omega \pm 5\%$, $\Delta FD = \pm 15\%$ and vice versa) it is possible to state the probability that the total damping is lower than the minimum value allowed by specifications.

As it is stated in the introduction, the results obtained with the Monte Carlo simulations can be summarized with the diagrams reported in Fig. 24a and b. As previously noted, the aeroelastic stability of the considered bridge is more sensible to variations of the frequencies than to a variation in the aerodynamic coefficients.

Considering the $\Delta\omega \pm 5\%$, $\Delta FD = \pm 15\%$ case (Fig. 24a), it is possible to make the following comments:

- total damping: the 25–75% percentile is within a 5% range of variation with respect to the nominal value for SLS1 and SLS2, while it is within a 10% range of variation for ULS and SILS. The 2.5–97.5% percentile is sufficiently far from the design limits.
- flutter velocity: the 25–75% percentile is within a 3% range of variation with respect to the nominal value, while for the 2.5–97.5% percentile it is within a 10% range.

Considering the $\Delta\omega \pm 15\%$, $\Delta FD = \pm 5\%$ case (Fig. 24b), it is possible to make the following comments:

- total damping: the 25–75% percentile satisfies the specifications, while the 2.5–97.5% percentile, due to the strong

asymmetry towards small values of damping, can have occurrences that overcame the minimum threshold.

- flutter velocity: both the 25–75% percentile and the 2.5–97.5% percentile are larger than the design wind velocity.

This last result highlights that, for a complete analysis of the aeroelastic stability, besides the flutter velocity, it is necessary also to evaluate the trend of the total damping.

4. Conclusions

In this paper we presented a statistical approach to study the aeroelastic stability of a suspended bridge, taking into account the effect of the variations from the nominal values of both mechanical and aerodynamic properties of the bridge. The mathematical and statistical background of the method were presented and the Messina Straits Bridge was analyzed as a test case.

The aeroelastic stability is studied not only analyzing the critical flutter velocity, but also the total damping as a function of the mean wind velocity. As a matter of fact, it has been shown that configurations with similar flutter velocities may have a different trend of the total damping.

The methodology requires the knowledge of the statistical distribution of the parameters with uncertainties, and it allows one to get the distribution of the total damping and flutter speed as a result. For the considered test case, we considered the uncertainty of the most relevant aerodynamic parameters and of the structural modal parameters. The method can be applied to any suspended bridge, but the results refer to the case analyzed due to the complexity of the aeroelastic problem.

The proposed approach can be a versatile design tool to compare different solutions when designing a new bridge, allowing the designer to indicate the most reliable one, given probability distribution of its aerodynamic or structural characteristics.

References

Argentini, T., Belloli, M., Fossati, F., Rocchi, D., Villani, M., 2011. Experimental and numerical analysis of the dynamic response of cable-stayed bridge: vortex induced vibrations and buffeting effects. In: The 13th International Conference on Wind Engineering. IAWQ, Amsterdam, The Netherlands.

Argentini, T., Diana, G., Larsen, A., Pagani, A., Portentoso, M., Somaschini, C., Yamasaki, Y., 2013. Comparisons between wind tunnel tests on a full aeroelastic model and numerical results of the Izmit bay bridge. In: The 6th European African Conference on Wind Engineering, Cambridge UK.

Baldomir, A., Hernández, S., Nieto, F., Jurado, J., 2011. Reliability analysis of flutter speed in long span bridges using form technique. In: ICWE 13, Amsterdam.

Baraldi, P., Popescu, I., Zio, E., 2010. Methods for uncertainty analysis in the reliability assessment of a degrading structure. In: SRA into SRA: structural reliability analyses into system risk assessment. Det Norske Veritas AS.

Bartoli, G., Mannini, C., 2005. Reliability of bridge deck flutter derivative measurement in wind tunnel tests. In: ICOSSAR 2005.

Bucher, C.G., Lin, Y.K., 1988. Stochastic stability of bridges considering coupled modes. *J. Eng. Mech.* 114, 2055–2071.

Chen, X., 2007. Improved understanding of bimodal coupled bridge flutter based on closed-form solutions. *J. Struct. Eng.* 133, 22–31.

Chen, X., Kareem, A., Matsumoto, M., 2001. Multimode coupled flutter and buffeting analysis of long span bridges. *J. Wind Eng. Ind. Aerodyn.* 89, 649–664.

Chen, X., Matsumoto, M., Kareem, A., 2000. Aerodynamic coupling effects on flutter and buffeting of bridges. *J. Eng. Mech.* 126, 17–26.

Cheng, J., Cai, C.S., Xiao, R.C., Chen, S.R., 2005. Flutter reliability analysis of suspension bridges. *J. Wind Eng. Ind. Aerodyn.* 93, 757–775.

Cheng, J., Li, Q.S., 2009. Reliability analysis of long span steel arch bridges against wind-induced stability failure. *J. Wind Eng. Ind. Aerodyn.* 97, 132–139.

Çevik, M., Pakdemirli, M., 2005. Non-linear vibrations of suspension bridges with external excitation. *Int. J. Non-Linear Mech.* 40, 901–923.

Diana, G., Falco, M., Bruni, S., Cigada, A., Larose, G., Damsgaard, A., Collina, A., 1995. Comparisons between wind tunnel tests on a full aeroelastic model of the proposed bridge over Stretto di Messina and numerical results. *J. Wind Eng. Ind. Aerodyn.* 54–55, 101–113.

Diana, G., Resta, F., Zasso, A., Belloli, M., Rocchi, D., 2004. Forced motion and free motion aeroelastic tests on a new concept dynamometric section model of the messina suspension bridge. *J. Wind Eng. Ind. Aerodyn.* 92, 441–462.

Diana, G., Rocchi, D., Argentini, T., 2013a. An experimental validation of a band superposition model of the aerodynamic forces acting on multi-box deck sections. *J. Wind Eng. Ind. Aerodyn.* 113, 40–58.

Diana, G., Yamasaki, Y., Larsen, A., Rocchi, D., Giappino, S., Argentini, T., Pagani, A., Villani, M., Somaschini, C., Portentoso, M., 2013b. Construction stages of the long span suspension Izmit bay bridge: wind tunnel test assessment. *J. Wind Eng. Ind. Aerodyn.* 123, 300–310.

Dyrbye, C., Hansen, S.O., 1997. *Wind Loads on Structures*. John Wiley & Sons.

Ge, Y.J., 2011. Challenging aerodynamic concerns of cable-supported bridges with super long span. In: The 13th International Conference on Wind Engineering. IAWQ, Amsterdam, The Netherlands.

Ge, Y.J., Xiang, H.F., Tanaka, H., 2000. Application of a reliability analysis model to bridge flutter under extreme winds. *J. Wind Eng. Ind. Aerodyn.* 86, 155–167.

Jakobsen, J.B., Tanaka, H., 2003. Modelling uncertainties in prediction of aeroelastic bridge behaviour. *J. Wind Eng. Ind. Aerodyn.* 91, 1485–1498.

Kiureghian, A.D., 2005. First and second order reliability methods. In: *Engineering Design Reliability Handbook*. CRC Press, Boca Raton, FL.

Mannini, C., Bartoli, G., 2010. The problem of uncertainty in the measurement of aerodynamic derivatives. In: *Safety, Reliability and Risk of Structures, Infrastructures and Engineering Systems*, pp. 824–831.

Matsumoto, M., Kobayashi, Y., Shirato, H., 1996. The influence of aerodynamic derivatives on flutter. *J. Wind Eng. Ind. Aerodyn.* 60, 227–239.

Matsumoto, M., Matsumiya, H., Fujiwara, S., Ito, Y., 2010. New consideration on flutter properties based on step-by-step analysis. *J. Wind Eng. Ind. Aerodyn.* 98, 429–437.

Ostenfeld-Rosenthal, P., Madsen, H.O., Larsen, A., 1992. Probabilistic flutter criteria for long span bridges. *J. Wind Eng. Ind. Aerodyn.* 42, 1265–1276.

Prenninger, P.H.W., Matsumoto, M., Shiraishi, N., Izumi, C., Tsukiyama, Y., 1990. Reliability of bridge structures under wind loading. Consideration of uncertainties of wind load parameters. *J. Wind Eng. Ind. Aerodyn.* 33, 385–394.

Pourzeynail, S., Datta, T.K., 2002. Reliability analysis of suspension bridges against flutter. *J. Sound Vib.* 254, 143–162.

Qin, Q., Li, H.B., Qian, L.Z., 2001. Modal identification of Tsing Ma bridge by using improved eigensystem realization algorithm. *J. Sound Vib.* 274, 325–341.

Scanlan, R., Jones, N., Singh, L., 1997. Inter-relations among flutter derivatives. *J. Wind Eng. Ind. Aerodyn.* 69–71, 829–837.

Zasso, A., 1996. Flutter derivatives: advantages of a new representation convention. *J. Wind Eng. Ind. Aerodyn.* 60, 35–47.

Zasso, A., Stoyanoff, S., Diana, G., Vullo, E., Khazem, D., Pagani, K.S.A., Argentini, T., Rosa, L., Dallaire, P.O., 2013. Validation analyses of integrated procedures for evaluation of stability, buffeting response and wind loads on the messina bridge. *J. Wind Eng. Ind. Aerodyn.* 122, 50–59.

Zio, E., Marsegua, M., 2002. Basics of the Monte Carlo Method with Application to System reliability. Lilole Verlag GmbH.